Available online www.jocpr.com

Journal of Chemical and Pharmaceutical Research, 2015, 7(4):1323-1331

Research Article

ISSN : 0975-7384
CODEN(USA) : JCPRC5

Sensitivity Research of the Unsteady Aerodynamics of a Horizontal Axis Wind Turbine under Different Yaw Angle

Xiaoming Chen and Shun Kang

School of North China Electric Power University, Key Laboratory of CMCPPE Ministry of Education, Beijing 102206, China

---

ABSTRACT

For an accurate analysis of the influence of yaw angle on the aerodynamic characteristics of the NREL Phase VI horizontal axis wind turbine (HAWT), the three-dimensional unsteady computational fluid dynamics (CFD) method in sliding grid technique is used in the simulation. In a case of 7 m/s flow velocity and 0° yaw angle, a comparison of the aerodynamic power and pressure coefficient is carried out between the CFD result and the experiment result, which validates our method. On the basis of this method, at the same flow velocity, different yaw angles are chosen to research the impacts of yaw angle on the aerodynamic characteristics of an HAWT. Meanwhile, the change of rules of aerodynamic power and 3D flow at different azimuthal angles are studied. Furthermore, the influence of different yaw angles on the sensitivity of unsteady aerodynamics is investigated.

Keywords: Yaw angle, HAWT, Unsteady, Aerodynamic characteristic, Sensitivity.

INTRODUCTION

Wind energy is a clean energy and has the fastest-growing prospects for large-scale development and commercialization[1,2]. Horizontal-axis wind turbines (HAWTs) have been the most commonly used form of wind power equipment, and their sustained and rapid growth is expected to show that by 2015 the world wind power capacity will reach 450 million kilowatts, and in 2020 it will reach 1 billion kilowatts[3]. However, in the process of the wind turbine operation in the real wind field, all sorts of complex wind conditions are encountered, for example, the flow between the wind speed and axial angle; this phenomenon is called yaw. With the continuously increasing scale of HAWTs, more and more attention is being given to the impact of yaw on the capacity, output power and structural vibration of a wind turbine[4]. Hence, studying yaw plays an important role.

The flow in wind turbines, even in very large ones, is still essentially incompressible, with Mach numbers based on blade tip speed rarely exceeding 0.25. This fact justifies the use of incompressible fluid solvers for most wind turbines. Methods of various levels of complexity to predict the aerodynamic behaviour of a wind turbine rotor have been developed. Nowadays, methods of pneumatically analysing horizontal-axis wind turbines can be divided into two kinds: experimental and numerical methods. Because of the limitations of wind field experiments, numerical techniques are more popular in yaw analysis. Barnsley and Narramore[5,6] have researched the dynamic stall in a wind turbine by means of the computational fluid dynamics (CFD) method. Using the Navier-Stokes equations (N-S equations), Duque[7] obtained the pressure of a blade surface, which coincided fairly well with the experiment results. Meanwhile, Voutsinas[8] focused on the flow field under yaw using the CFD method. Xu and Sankar[9,10] also proposed a promising method that involved solving the N-S equation by the CFD approach in a small area around the turbine blade and by vortex theory in the other areas. The results have provided lots of references for the design and operation of HAWTs.

Although most studies assume the generated grid is static in the whole calculation process so as to greatly reduce the computational complexity and cost, for wind turbine blades, the detailed analysis near the rotating planar flow in the

flow field is affected. This article will use the URANS method of three-dimensional unsteady numerical simulation and verification in a NREL Phase VI wind turbine as the object, and will explore the wind speed (7 m/s) under the condition of axial flow and yaw with continuous three-dimensional unsteady flow characteristics of an HAWT, and the results are compared with experimental data and analysed in detail.

NUMERICAL METHODS

Description of the numerical example

The objective of the present research effort is to validate a first-principles-based approach for modelling HAWTs under yawed flow conditions using NREL Phase VI rotor data [11-14].Geometric parameters are shown in Table 1.
Experiments through the arrangement of pressure holes at the five sections of 30%, 47%, 63%, 47% and 63% in the blade measure the blade surface pressure, tangential force and normal force coefficient along with chordwise. In this paper, a 3D aerodynamic characteristics analysis model is used under the following conditions of blade pitch. Angle is 4.815 °, 7 m/s wind speed, the yaw angles are 0 °, 15 °, 30 °, 45 ° and 60 °, the calculation results are compared with the experimental model to confirm the calculation model.

Table 1 Geometric parameters of a NREL Phase Ⅵ wind turbine

Type	Parameters
Number of blades,Z	2
airfoil	S809
Rotor radius,R	5．029m
Rotor speed,N	71.6r/min
Hub radius,R	0.508m
Tip Angle of pitch	4.815°

Computational domain

The computational domain has a height of 30.2 m (6R) and a width of 30.2 m, corresponding to a 30.2 m * 30.2 m wind tunnel, with a length of 90 m（18R）in the stream-wise direction. The wind turbine is placed approximately in the middle of the wind tunnel at a distance of 6R from the upwind boundary. The computational domain for the wind turbine placed in the wind tunnel is illustrated in Fig. 1. The domain consists of two parts, namely the moving parts (cylinder and rectangle part) and the stationary part (wind tunnel part). The wind turbine is placed approximately in the middle of the moving parts, which are a 15.1 m (3R) diameter circle with a length of 5.03 m（1R）in the stream-wise direction.

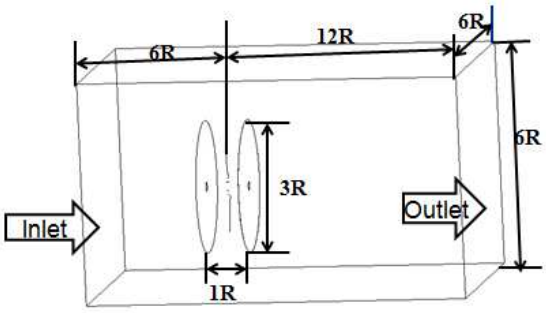

Fig. 1 Computational domain

The grid division

A grid with a total of 6.3 million elements in the computational domain was modelled by the Fluent software package under the ICEM's 1.3 million elements and the rotating domain was simulated automatically by the NUMECA software package using the grid mesh generator AutoGrid5 B2B CUT function for 5 million grid elements, as shown in Figure 2 (a), which illustrates the distribution of the grid computational and rotating domains. The grid distribution around the rotor blade is shown in Figure 2 (b). The rectangle surrounding the two blades was composed of O4H grid topology meshes with 20 inflation layers on the blade surface, with a spacing ratio of 1.1 in the normal direction and a first height of 0.03 mm in order to accurately capture the boundary layer region. Y+ value was set to approximately one at the blade tip and decreased towards the blade root, which meets the needs of the turbulence model.

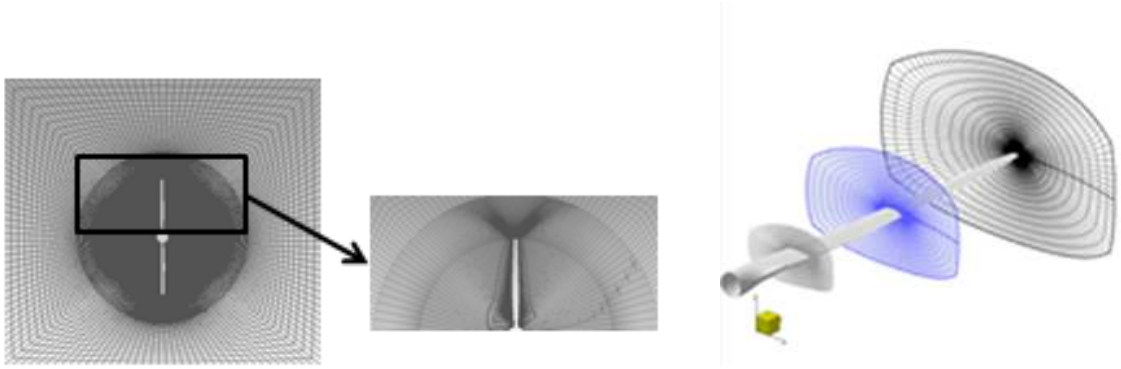

(a) (b)

Fig. 2 Meshing of three-dimensional model

The boundary conditions

A uniform velocity condition of 7 m/s was applied as the boundary condition at the inlet where the flow enters the computational domain. For the outlet where the flow leaves the domain, the ambient domain condition was selected. Wall condition was applied at the walls of the tunnel, ground and surfaces of the wind turbine whereas pressure condition with ambient pressure was applied at the downstream. The grid computing domain is stationary, and the sliding mesh method is adopted for stator domain interface data transfer.

Numerical methods

The commercial software Fluent is adopted to improve the Reynolds-averaged Navier-Stokes equation (RANS) and unsteady Reynolds-averaged Navier-Stokes equation (URANS) calculation. For the unsteady calculation, the software adopts the dual time-step approach to solve the URANS and the time integration method of the Krylov-type methods. As shown in Figure 3, for aerodynamic power calculation using the Spalart-Allmaras (SA) and K-e two turbulence model, compared with the experimental value it can be seen that the calculated results of the SA turbulence model are closer to the experimental value, so this research uses an SA turbulence equation model. In the three-dimensional model of the unsteady calculation, the physical time step adopted corresponds to an angle of 9°.

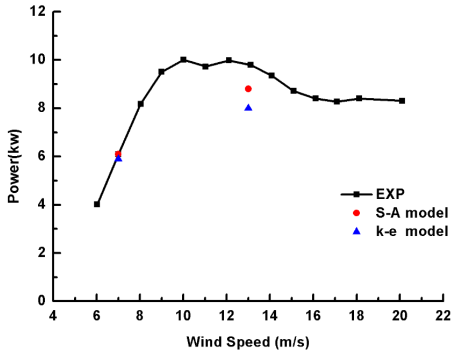

Fig. 3 Aerodynamic power curves change with wind speed

RESULTS AND DISCUSSION

Confirmation of the numerical methods

CFD calculation results with experimental values under the condition of 7 m/s and 0° yaw angle are shown in Figures 4. Among them, the "CFD" gave numerical results of the Fluent software, with "EXP" as the experimental value, and the following chart is the same. The results show that the tangential force coefficient, normal force coefficient and the pressure coefficient distribution of each section are in line with CFD calculation value and experimental value, proving that this method of CFD analysis is reasonable and reliable.

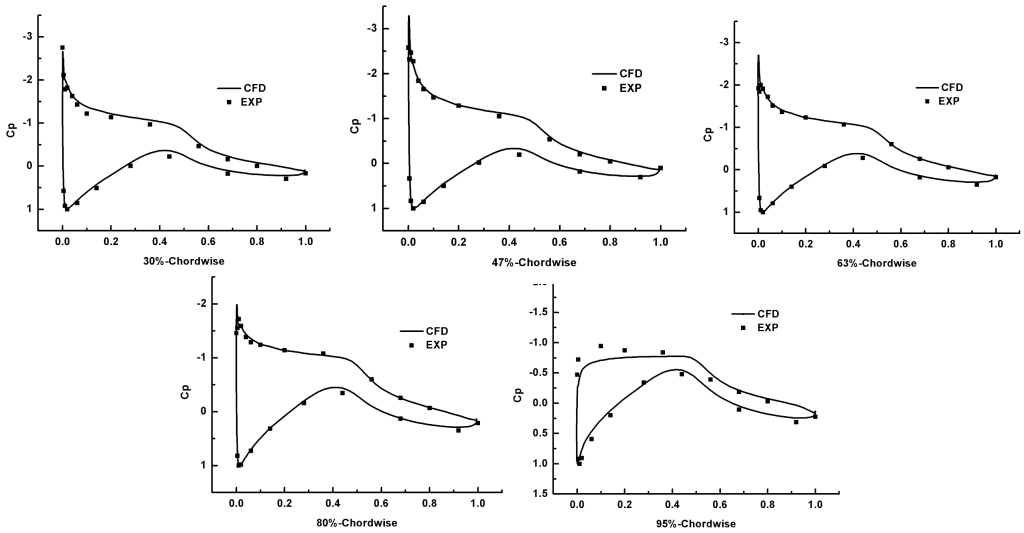

Fig. 4 The pressure coefficient at the different interfaces at 0° yaw angle

Aerodynamic characteristics under yaw condition

Torque changes along with azimuth angles under the condition of 7 m/s and 30° yaw angle are shown in Figure 5(a). It is possible to see an obvious periodicity, which is due to the angle of attack in a rotating cycle similar to the change of the sine curve, which causes a periodic change of the rotor induction; in Figure 5 (b), which shows the torque curve, it can be seen that the torque is in decline along with the change of yaw angle, and in 10° to 60° the rate of torque change is nearly linear. So Torque varies with the yaw angle, and it is more sensitive at the yaw angle less than 10 degree than at the yaw angle between 10 degree and 60 degree.

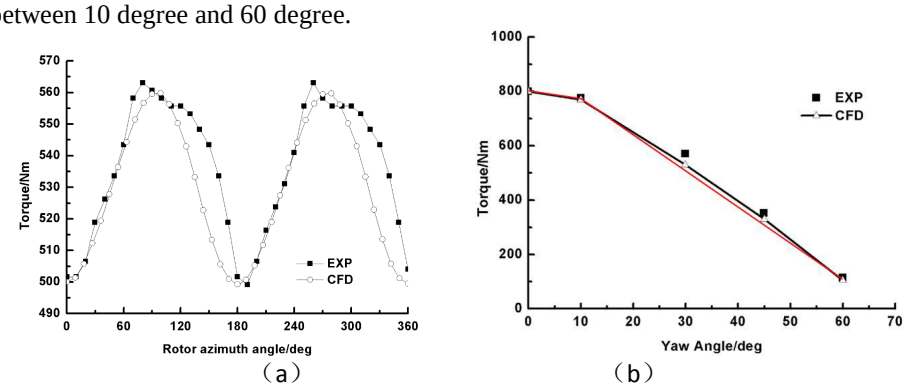

Fig. 5 The torque load with yaw angle and azimuthal angles at 30° yaw angle

Flow field analysis

Yaw flow direction is along the z axial partial x positive angle to 30 degrees as shown in Figure 6. In the XY plane rotate anticlockwise to the 12 o'clock position and set 0 degrees. At the 9 o'clock position set 90 degrees. At the 6 o'clock position set 180 degrees. At the 3 o'clock position set 270 degrees. Figure 7 shows a comparison of limiting streamlines at the different direction angles and different sections between yaw flow and uniform flow. It shows that under the circumstance of the constant yaw angle, the attach angle reached its peak at 0 degrees azimuth, corresponding to the largest separation zone, and the attach angle hit the bottom at the direction of 180 degrees azimuth with the smallest separation zone. Because of the same attach angle between 90 and 270 degrees azimuth, the positions of the separation line are very similar. However, since a velocity component along the blade tip to the blade root is generated by the influence of the yaw at the direction angle of 90 degrees, there is a corresponding velocity component from blade root to blade tip at 270 degrees azimuth. So from the leading edge to the trailing edge of the upper part of the blade, there are huge differences in the streamline gradient. The change of blade separation line is mainly concentrated on the lower part of the blade, which causes the cyclical fluctuations of aerodynamic forces. As the yaw angle increases, the changes of attach angle at the different direction angles are more and more fierce. Noticeable changes are also found in the blade root separation zone position, with the corresponding limiting streamline also being affected. From the qualitative analysis of the flow pressure distribution at the 30% section, there is an obvious change in different yaw angle, while qualitative analysis of other sections does not see a very obvious change. We can infer that 0 degrees

azimuth is more sensitive to separation. So Figure 7 shows the coefficient of the pressure distribution curve of different yaw angles under different azimuths and different sections. From the plot, in the same section of constant yaw angle, due to changes of azimuth angle, the pressure coefficient curves are not the same. The pressure coefficient curves at the 90 and 270 degree azimuth angles at the pressure surface are in good agreement while the suction surface is only a bit different at the trailing edge. This is consistent with the preceding analysis. In the same azimuth angle and section, as the yaw angle increases, the pressure coefficient changes a lot. From the pressure coefficient curves of each section, with either a change of the yaw angle or change of the azimuth, the closer to the blade tip, the smaller the effect the change of the pressure coefficient curve has. Namely, much closer to the blade tip has a lower sensitivity to the yaw effect. The phenomena provide a foundation for a separation strategy study on active control.

Figure 8 shows the iso-surface graph of the vortical structure at Q=1 and wake axial velocity contour at the wind wheel 0.8R distance. The only change is seen with the yaw angle in the vortex structure iso-surface graph at the 0- and 180-degree azimuth. The length of the vortical structure is shorter at the 0-degree azimuth than at the 180-degree azimuth. However, it can clearly be seen that with the change of the yaw angle, the shift angle of the vortex structure due to the yaw influence is larger.

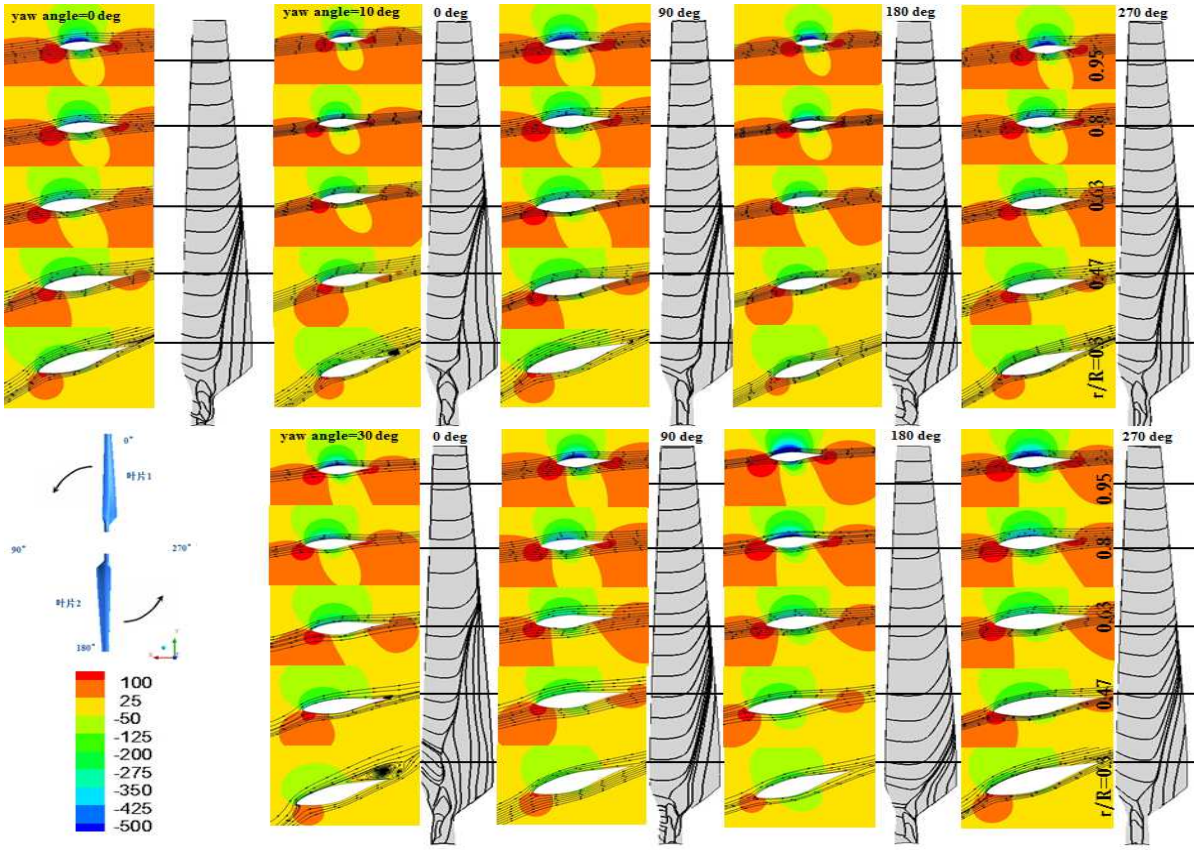

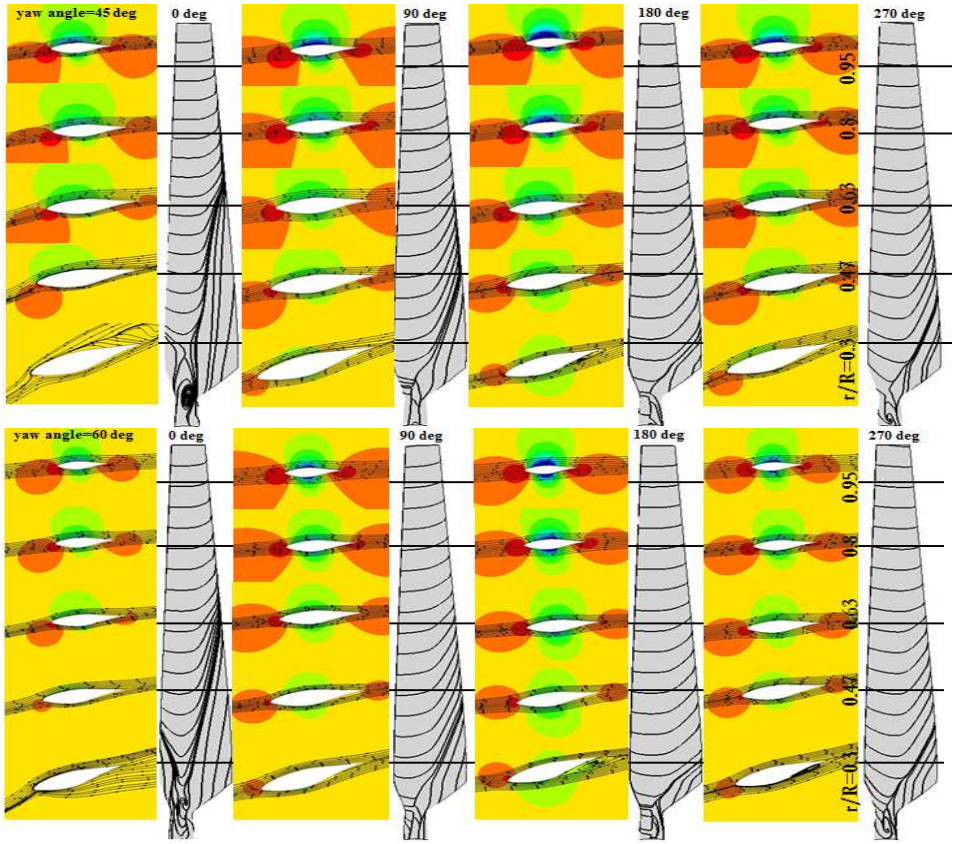

Fig.6 Pressure distribution at different sections and the streamline of blade at different angles at 7m/s

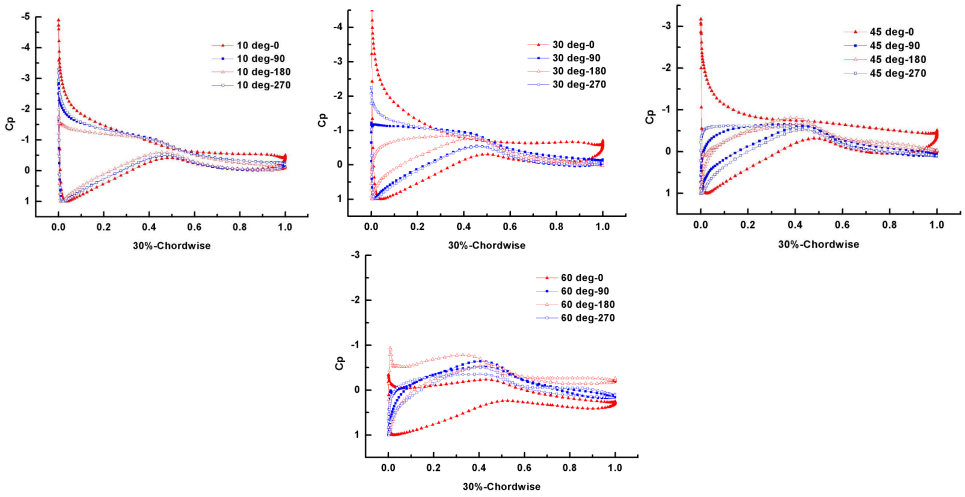

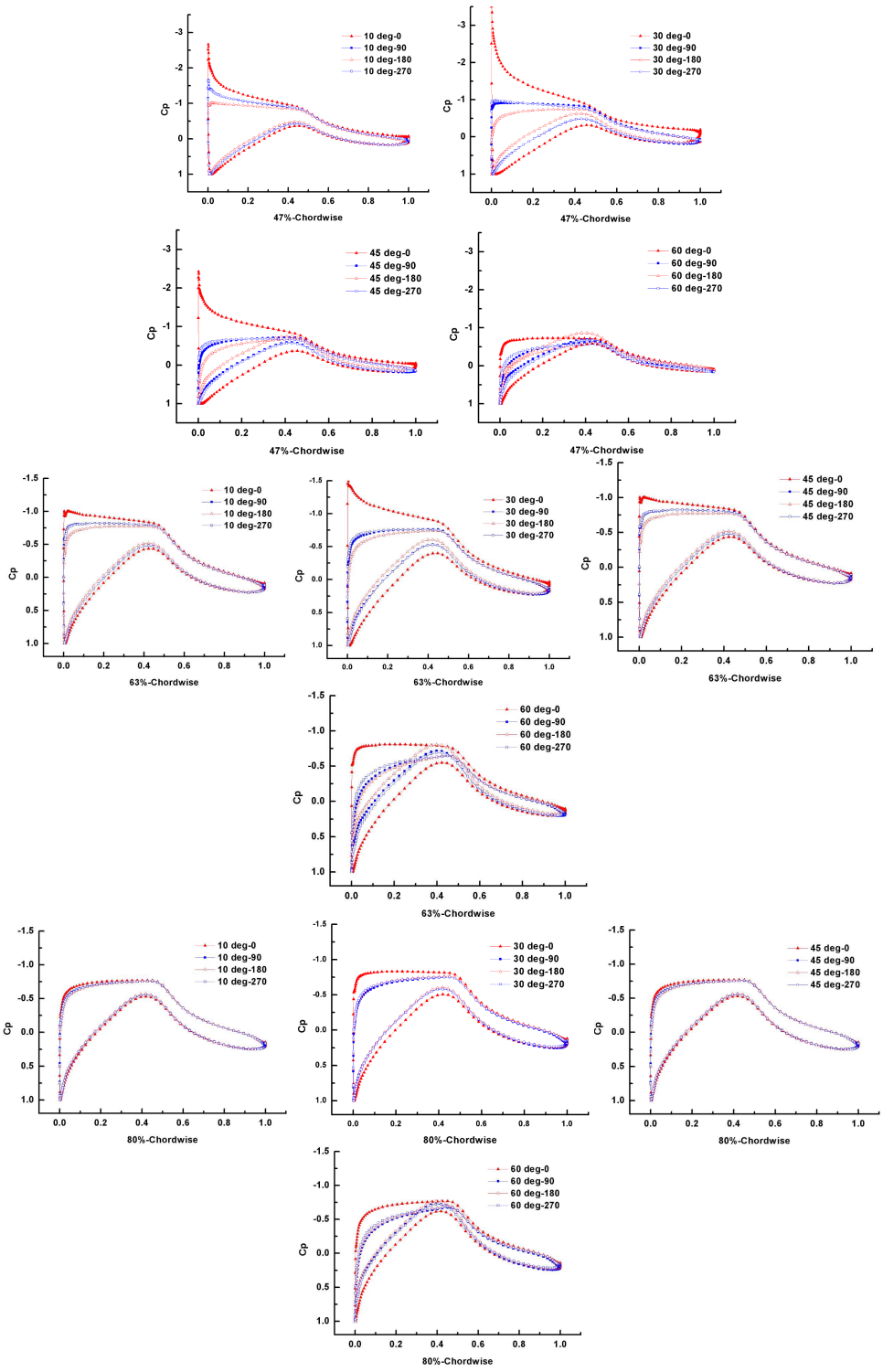
10 deg-0
10 deg-90
10 deg-180
10 deg-270
30 deg-0
30 deg-90
30 deg-180
30 deg-270
45 deg-0
45 deg-90
45 deg-180
45 deg-270
60 deg-0
60 deg-90
60 deg-180
60 deg-270
Cp
47%-Chordwise
63%-Chordwise
80%-Chordwise

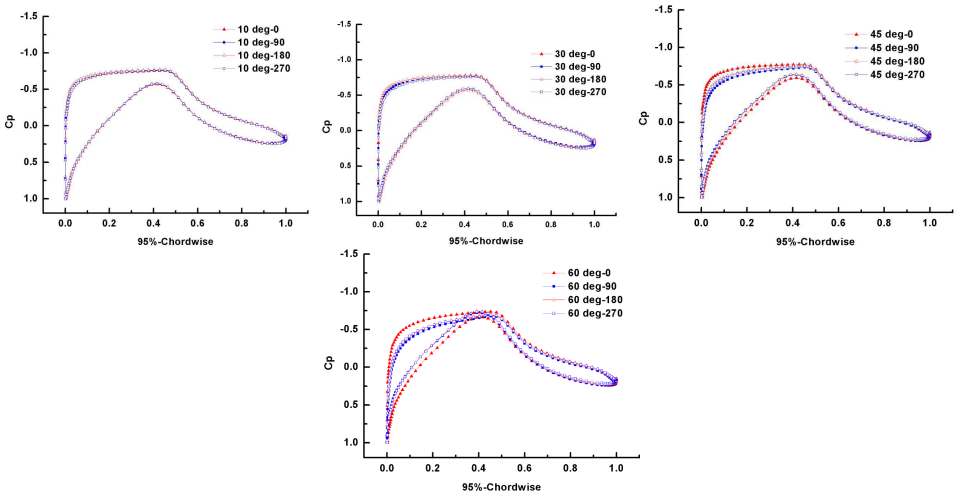

Fig. 7 The pressure coefficient at different interfaces and azimuthal angles under 10°、30°、45°and60°yaw angle

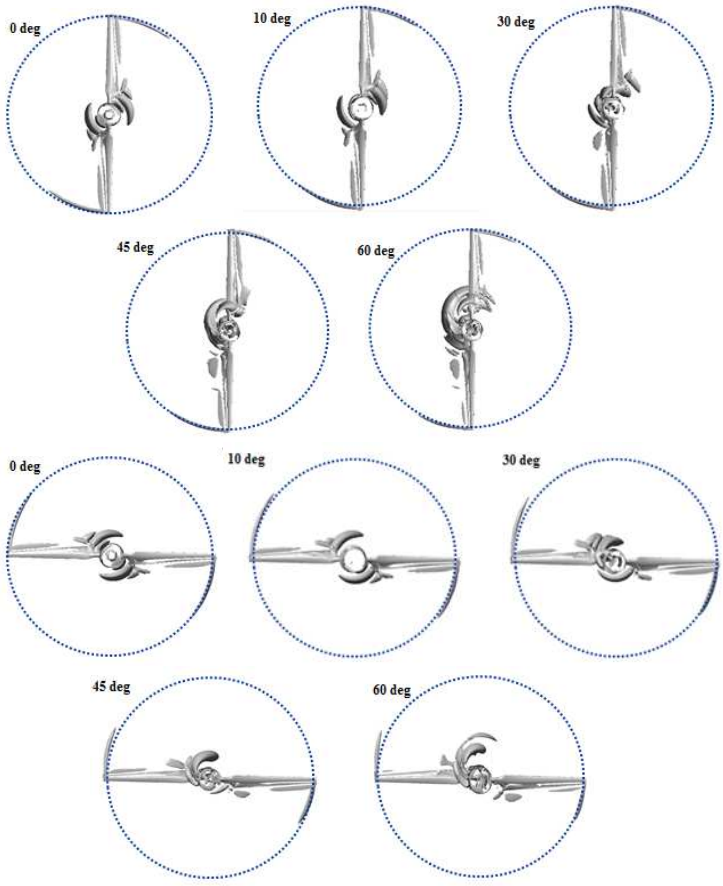

Fig. 8 Vortical structures are represented by iso-surfaces of Q =1

CONCLUSION

This paper established a three-dimensional unsteady CFD calculation method simulating wind turbine aerodynamic performance under yaw conditions, and the NREL Phase VI wind turbine is verified as an example. The conclusions drawn are as follows:

1. Under the condition of 0° yaw angle, simulation of HAWT aerodynamic performance reflects well the aerodynamic characteristics;

2, On other yaw condition, unsteady process is possible to see an obvious periodicity. With azimuth variation ,separation conditions are very different . Torque varies with the yaw angle, and it is more sensitive at the yaw angle less

than 10 degree than at the yaw angle between 10 degree and 60 degree; 0 degrees azimuth is more sensitive to separation; much closer to the blade tip has a lower sensitivity to the yaw effect, the phenomena provide a foundation for a separation strategy study on active control;
3,Under the circumstance of yaw,the change of the Q value corresponding to the increase of yaw angle is more sensi tive.Wake deviation and asymmetry is more subsceptible with the increase of the yaw angle.

Acknowledgments
This research was supported by National Natural Science Foundation of China (No.51176046) and the National 863 high technology research and development plan project (2012AA051303).

REFERENCES

[1] Jang-Oh Mo, Amanullah Choudhry, Maziar Arjomandi and Young-Ho Lee. L. *Journal of Wind Engineering and Industrial Aerodynamics*,**2013**,112：11–24.
[2] Archer CL. *Journal of Geophysical Research* **2005**;110:D12110.
[3] Global Wind Energy Council. Global Wind Report-Annual market update 2010[R]
[4] Fadaeinedjad R, Moallem M. *IEEE Transactions on Energy Conversion*, **2009**, 24(1)
[5] M. J. Barnsley，J. F. Wellicome. *Journal of Wind Engineering and Industrial Aerodynamics*，**1992**，39(1-3).
[6] J. C. Narramore，R. Vermelandt. *Journal of Aircraft*，**1992**，29(1)：73-78.
[7] E. P. N. Duque，C. P. Van Dam. Navier-Stokes simulation of the NREL combined experiment Phase II rotor[C]. Reno：34th AIAA Aerospace Sciences Meeting. **1999**.
[8] S. G. Voutsinas，J. P. Glekas，A. Zervos. *Journal of Wind Engineering and Industrial Aerodynamics*，1**992**，39(1-3)：293—30 1.
[9] G. Xu，L. N. Sankar. *Journal of Solar Energy Engineering*，**2000**，122(1)：35-39.
[10] G. Xu，L. N. Sankar. Application of a viscous flow methodology to the NREL Phase VI rotor[C]. ASME Conference Proceedings，**2002**，2002(7476X)：83-93.
[11] Hand M, Simms D, Fingersh L, etc. Unsteady Aerodynamics Experiment Phase VI: Wind Tunnel Test Configurations and Available Data Campaigns [R]. NREL/TP-500-29955, NREL, **2001**
[12] Simms, D. A., Schreck, S., Hand, M. M., and Fingersh, L. J, **2001**, "NRELUnsteady Aerodynamics Experiment in the NASA-Ames Wind Tunnel: A Comparison of Predictions to Measurements," NICH Report No. TP-500-29494.
[13] Fingersh, L. J., Simms, D. A., Hand, M. M., Jager, D. W., Cotrell, J. R.,Robinson, M., Schreck, S. and Larwood, S. M., **2001**, "Wind Tunnel Testing of NREL's Unsteady Aerodynamics Experiment," AIAA Pap. 2001-0035.
[14] Giguere, P., and Selig, M., **1999**, "Design of a Tapered and Twisted Blade for the NREL Combined Experiment Rotor," National Renewable Energy Laboratory,NREL/SR-500-26173, Golden, CO.